

Exploiting Fluorescence Lifetime Plasticity in FLIM: Target Molecule Localization in Cells and Tissues

A. Boreham,[†] T.-Y. Kim,[†] V. Spahn,[‡] C. Stein,[‡] L. Mundhenk,[§] A. D. Gruber,[§] R. Haag,^{||} P. Welker,[⊥] K. Licha,[⊥] and U. Alexiev^{*†}

[†]Institut für Experimentalphysik, Freie Universität Berlin, Arnimallee 14, D-14195 Berlin, Germany

[‡]Klinik für Anästhesiologie, Charité-Universitätsmedizin Berlin, Campus Benjamin Franklin, Hindenburgdamm 30, 12203 Berlin, Germany

[§]Institut für Tierpathologie, Freie Universität Berlin, Robert-von-Ostertag-Strasse 15, 14163 Berlin, Germany

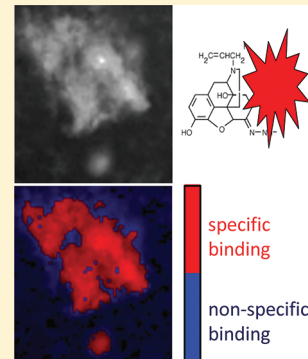
^{||}Institut für Chemie und Biochemie, Freie Universität Berlin, Takustrasse 3, 14195 Berlin, Germany

[⊥]mivenion GmbH, Robert-Koch-Platz 4, 10115 Berlin, Germany

S Supporting Information

ABSTRACT: The mechanisms of drug–receptor interactions and the controlled delivery of drugs via biodegradable and biocompatible nanoparticulate carriers are active research fields in nanomedicine. Many clinically used drugs target G-protein coupled receptors (GPCRs) due to the fact that signaling via GPCRs is crucial in physiological and pathological processes and thus central for the function of biological systems. In this letter, a fast and reliable ratiometric fluorescence lifetime imaging microscopy (rmFLIM) approach is described to analyze the distribution of protein–ligand complexes in the cellular context. Binding of the fluorescently labeled antagonist naloxone to the G-protein coupled μ -opioid receptor is used as an example. To show the broad applicability of the rmFLIM method, we extended this approach to investigate the distribution of polymer-based nanocarriers in histological liver sections.

KEYWORDS: G-protein coupled receptors, μ -opioid receptor, ligand binding, FLIM, nanocarrier



Fluorescence lifetime imaging (FLIM) is a technique that can be used to extract information about macromolecules from biological samples on the basis of the sensitivity of the spectral and temporal fluorescence properties to the physicochemical environment.¹ In combination with Förster resonance energy transfer (FRET) FLIM is a widely used method to map protein–protein interactions on the nanometer-scale in living cells.^{1–3} Genetically encoded fluorescent proteins expressed as fusions with the target proteins are predominantly used as donor and acceptor molecules within living cells.⁴ The use of organic fluorophores is less common in this type of experiment. In the case of membrane receptors or intracellular proteins that bind extracellular ligands, however, organic fluorophores are the dye of choice to label the ligand.^{5–7} Fluorescence intensity based imaging methods are often used to localize the cellular sites where the ligand binds to its cognate receptor,^{6,8} but these techniques may be biased by unspecific binding and distribution of the ligand in various subcellular compartments. Here again, FLIM measurements may provide an advantage based on the sensitivity of the fluorescence lifetime properties to the physicochemical environment. We show in this letter a fast and reliable FLIM based method for localization of target molecules and their discrimination against the fluorescent background of cell membranes and tissue.

FRET measured via fluorescence lifetime relies on the shortening of the donor lifetime due to the radiationless energy

transfer to the acceptor.² However, not only FRET but also the physicochemical environment including other quenching processes may affect the fluorescence lifetime. A shortening of the fluorescence lifetime is seen, for instance, in the case of static and dynamic quenching by quencher molecules or for photo-induced energy transfer processes based on the interaction of organic dyes with tryptophan.⁹ We recently detected that binding of an organic fluorophore to the protein matrix of the GPCR rhodopsin via a reactive cysteine residue also resulted in a significant decrease of the fluorescence lifetime of the bound fluorophore compared to the unbound fluorescent dye.^{10–12} The time-resolved fluorescence was measured by using time-correlated single photon counting, and the decay curves obtained were fitted to a number of exponential functions.^{10,13} Figure 1A–C shows the fluorescence lifetime curves of fluorescein (Flu) free in solution, fluorescein bound to cysteine (Cys-Flu), and fluorescein bound to Cys316 in the opsin molecule (Opsin-Cys316-Flu). While covalent binding of fluorescein to the small molecule cysteine results only in a marginal change of the fluorescence lifetime curve (Figure 1B), the quenching effect is clearly visible for Opsin-Cys316-Flu (Figure 1C). The data were significantly better fitted by using multiexponentials compared with one.

Received: April 7, 2011

Accepted: August 9, 2011

Published: August 09, 2011

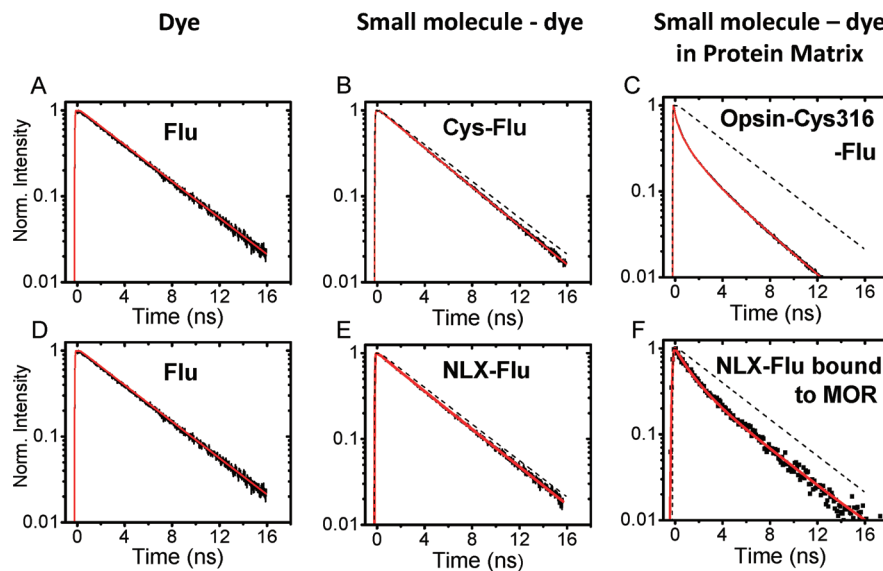


Figure 1. Fluorescence lifetime curves in dependence of environment. (A and D) fluorescein free in solution (Flu; 1 μ M); (B) fluorescein covalently bound to cysteine (Cys-Flu; 2 μ M); (C) fluorescein bound to the protein matrix of opsin via cysteine 316 (Opsin-Cys316-Flu; 5 μ M; 20–30% labeling stoichiometry); (E) fluorescein covalently coupled to naloxone (NLX-Flu; 1.2 μ M); and (F) NLX-Flu (1.2 μ M) bound to MOR expressed in HEK293 cell membranes. Dashed lines in parts B, C, E, and F indicate the lifetime decay of free fluorescein. Red lines are exponential fits to the measurement data. Fit results are summarized in Table 1 of the Supporting Information. Conditions: 150 mM NaCl, pH 7.5, 20 °C. Fluorescence excitation was at 485 nm; emission was detected with color cutoff filter OG515 or a band-pass filter 500–550 nm.

In addition to the decrease of the 4 ns fluorescence lifetime component of free fluorescein to 3.6 ns, two shorter decay components with 74% of the total amplitude were extracted from the fit. Here, the shortening of the fluorescence lifetime results from additional dynamic interaction of the bound dye with the surrounding protein matrix, which functions as a quencher.

On the basis of this observation, we propose, in analogy to FRET-FLIM, a ratiometric FLIM (rmFLIM) approach, which relies on the specific multiexponential lifetime signature of a protein–ligand complex that is unique compared to the fluorescence lifetime distribution of the background. An advantage over FRET-FLIM is that only one fluorophore is needed.

We tested the rmFLIM approach for the analysis of μ -opioid receptor (MOR) expression and ligand binding in human embryonic kidney (HEK)-293 cells, a widely used system for transfection and mutagenesis of GPCR.¹⁴ The human MOR plays a central role in the modulation of pain perception and mediates the analgesic and addictive properties of opiate drugs, including morphine.¹⁵ The commonly used assay for ligand binding to the expressed opioid receptors is based on the binding of radioligands.¹⁶ Radioactivity in the extracted cell or tissue fractions is measured by scintillation counting. The advantage of the proposed rmFLIM approach is 2-fold: (1) Fluorescence instead of radioactivity is used as readout, and (2) not only ligand binding but also the subcellular distribution of the expressed receptor to which the ligand binds can be spatially resolved in a single step without further time-consuming sample preparation and washing steps. As a ligand we used the MOR antagonist naloxone coupled to fluorescein (NLX-Flu). Figure 1D–F shows the fluorescence lifetime curves of fluorescein (Flu) free in solution, NLX-Flu, and NLX-Flu bound to MOR. The lifetime curves were obtained by time-correlated single photon counting within a confocal laser scanning FLIM setup consisting of an Olympus IX71 microscope equipped with a 40 \times objective lens, a

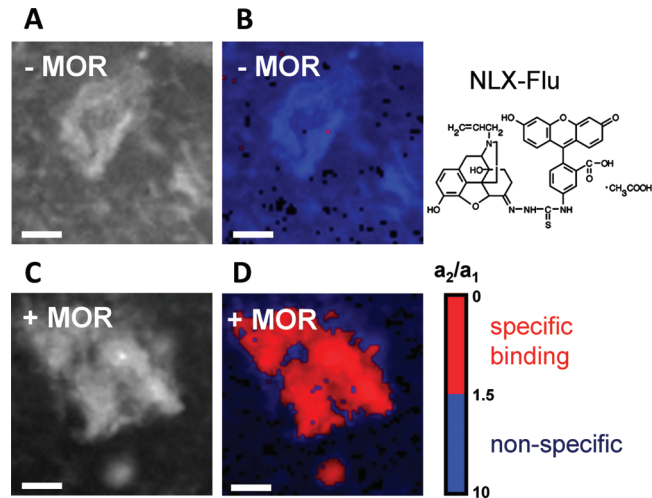


Figure 2. rmFLIM of NLX-Flu binding to MOR expressed in HEK293 cell membranes. (A) Fluorescence intensity image of membrane fragments from untransfected HEK293 cells (-MOR) incubated with NLX-Flu (1.2 μ M). (B) rmFLIM image for data shown in part A. False color coding based on the amplitude ratio a_2/a_1 of the two fluorescein lifetime components obtained from a global fit with $\tau_1 = 1$ ns and $\tau_2 = 4$ ns. The structure of NLX-Flu is shown. (C) Intensity image of membrane fragments from HEK cells expressing MOR incubated with NLX-Flu (1.2 μ M). (D) rmFLIM image of part C with false color coding. Conditions: 150 mM NaCl, 5 mM Tris pH 7.5, 20 °C. Fluorescence excitation was at 485 nm; emission was detected with a band-pass filter 500–550 nm. Scale bar: 20 μ m.

confocal scanning unit (DCS-120, Becker & Hickel, Berlin, Germany), and a Ti:sapphire Tsunami laser pumped by a solid state Millenia V laser (Spectra Physics) in the mode-locked picosecond-pulsed regime. The fluorescence lifetime curve of NLX-Flu is similar to that of free fluorescein. The effect is

comparable to the binding of fluorescein to cysteine, as both cysteine and naloxone can be viewed as small molecules to which the dye is covalently bound. As expected from the results with opsin (Figure 1C), binding of NLX-Flu to MOR results in a fluorescence lifetime curve that exhibits multiexponential decay behavior (Figure 1F). In addition to the 4 ns fluorescence lifetime component of free fluorescein, a 1 ns decay component with 55% of the total amplitude was extracted from the fit. Although the quenching effect mediated through the protein matrix is overall similar for both opsin and MOR, the differences in fluorescein lifetimes and corresponding amplitudes are attributed to the specific protein or protein/membrane environments. To discriminate between MOR-bound NLX-Flu and nonspecific binding in the FLIM images of HEK293 cell membranes (Figure 2), we used global fluorescence lifetime fitting with two lifetimes of 1.0 and 4.0 ns. As the 4 ns lifetime component is reduced in its relative amplitude from 91% to 45% upon specific binding to MOR, we color-coded the image pixels according to the ratio of the relative amplitudes of the two lifetime components from the global fit. For free NLX-Flu the ratio between the amplitudes of

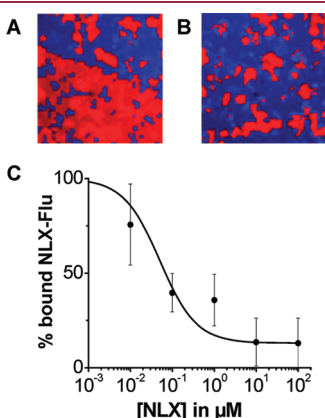


Figure 3. Displacement of NLX-Flu by NLX in rmFLIM images. (A) and (B) rmFLIM image of MOR containing cell membranes with NLX-Flu ($1 \mu\text{M}$) bound to MOR (red). (B) Addition of $0.1 \mu\text{M}$ nonfluorescent NLX to cell membranes shown in part A. Color coding is according to Figure 2. (C) Dose–response curve for displacement of NLX-Flu bound to MOR by nonfluorescent NLX. Data points represent the mean from five independent determinations. The standard deviation is given. The half-maximum concentration for displacement determined from the fit (solid line) is $0.05 \mu\text{M}$. Conditions as in Figure 2.

the two lifetime components (a_2/a_1) is about 10; for specific binding of NLX-Flu to MOR the amplitude ratio is about 0.8. As a threshold we used 1.5, which corresponds to 60% relative amplitude of the 4-ns-lifetime species. Values below 1.5 indicate specific binding and are colored in red, values between 1.5 and 10 indicate nonspecific interactions and are colored in blue. Figure 2 compares the fluorescence intensity based images with the FLIM images of HEK293 cells expressing MOR and control cells transfected with the empty expression vector. While in the fluorescence intensity based images the cell membranes of both cell types are visible due to specific and nonspecific binding of the hydrophobic ligand NLX-Flu, the rmFLIM images allow a clear-cut discrimination between specific and nonspecific ligand binding. The control HEK293 cell membranes in Figure 2B display a homogeneous blue coloring in the rmFLIM images. Cell membranes from HEK293 cells expressing MOR predominantly show specific binding of NLX-Flu to MOR, as indicated by the red coloring in the rmFLIM image (Figure 2D). The distribution of the ligand-bound receptor, however, is not homogeneous throughout the cell membrane, consistent with the concept of localization within lipid rafts.¹⁷ To verify the specific binding of NLX-Flu to MOR, we used unlabeled naloxone (NLX) in increasing concentrations to displace NLX-Flu from the receptor. Figure 3 shows a dose–response curve for the displacement of NLX-Flu. The increase of the fluorescence lifetime amplitude ratio (red to blue transition) within a selected membrane region, corresponding to the displacement of specifically bound NLX-Flu by unlabeled NLX, is shown in Figure 3A and B. The decrease of the amount of bound NLX-Flu as a function of increasing NLX concentrations in Figure 3C clearly shows the specific binding of NLX-Flu to the MOR expressing HEK293 cells and thus the applicability of our rmFLIM approach.

In a next step we extended the rmFLIM method to the analysis of the fate of a polymer based nanocarrier for drug delivery in the metabolic clearance process. We used a polyanionic, dendritic polyglycerolsulfate (dPGS) labeled with a fluorescent indocarbocyanine dye (ICC, spectrally analog to Cy3) as shown in Figure 4A,B.^{18,19} ICC in solution exhibits a fast fluorescence lifetime of 0.25 ns .²⁰ In its dPGS-conjugate state, however, the time-resolved fluorescence data were significantly better fitted by using two exponentials compared with one. In addition to a short decay component of 0.27 ns , we observed a longer fluorescence lifetime of 1.1 ns with a relative amplitude of 14% (Figure 4C). We assign the short-lifetime species to freely rotating ICC molecules,

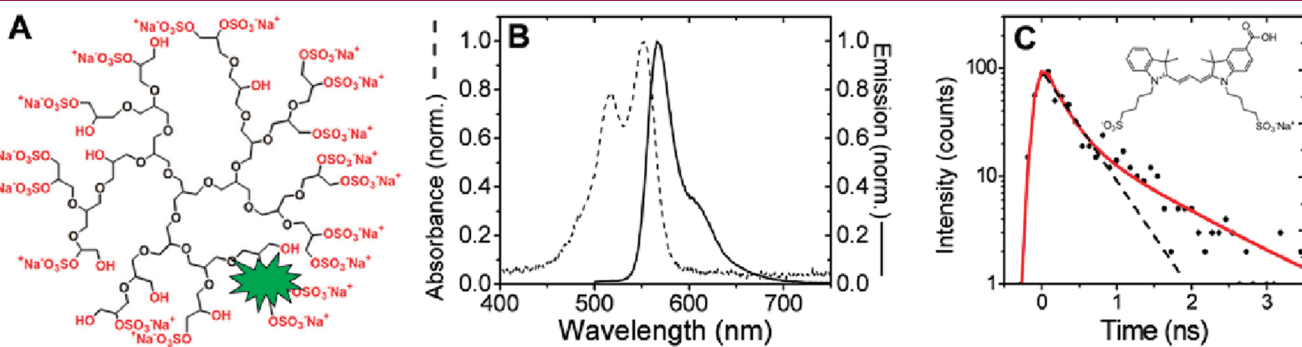


Figure 4. Fluorescence properties of ICC bound to dPGS. (A) Structure of dPGS;¹⁹ the green star represents the covalently bound fluorescent dye ICC (structure in inset of part C). (B) Absorption and emission spectra of dPGS-ICC. Fluorescence excitation was at 485 nm . (C) Fluorescence lifetime trace of dPGS-ICC. The dashed black line indicates the lifetime decay curve of the free ICC derivative used in the study. The red line is a biexponential fit to the data. Fit results are summarized in Table 1 (Supporting Information). Fluorescence excitation was at 485 nm ; emission was detected with a band-pass filter $590\text{--}650 \text{ nm}$. Conditions: 150 mM NaCl , $5 \text{ mM Tris pH } 7.5$, 20°C .

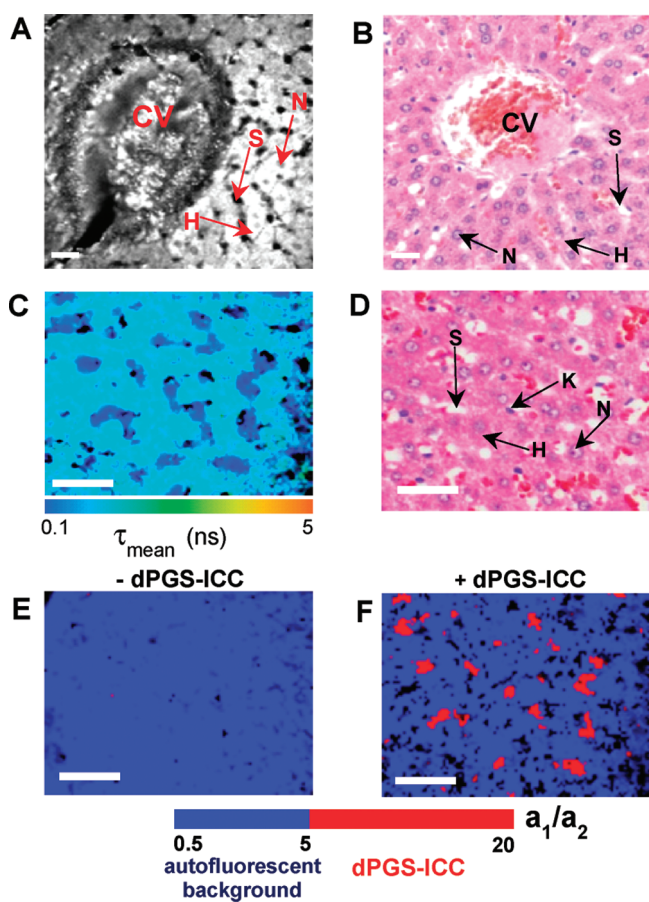


Figure 5. Discrimination of dPGS-ICC fluorescence against the auto-fluorescent background of liver tissue. (A) Autofluorescence of liver by confocal raster scanning microscopy. Excitation at 485 nm, emission filter HQ_{620/60} nm. In the histological liver section sinusoids (S) and hepatocytes (H) with nuclei (N) run toward the centrally located central vein (CV). Scale bar: 25 μ m. (B) Histological image of a liver section stained with hematoxylin and eosin at 1 μ m thickness from the same sample as in part A. The hepatocytes (H) are arranged radially in plates around the centrally located central vein (CV). Sinusoids (S) run between hepatic plates. The polygonal hepatocytes (H) contain a centrally located nucleus (N) surrounded by high amount of eosinophilic cytoplasm. Scale bar: 25 μ m. (C) FLIM image of a paraffin embedded rat liver tissue sample with dPGS-ICC morphologically corresponding to a region shown in part D. False color coding is based on the mean lifetime of a global lifetime fit with three components (measurement at 20 °C). Scale bar: 40 μ m. (D) Histological image stained with hematoxylin and eosin. Cells with small elongated spindle shaped nuclei of Kupffer cells (K) are located in the sinusoids (S) that clearly distinguish Kupffer cells from hepatocytes (H) with round vesiculated nuclei (N). Scale bar: 40 μ m. (E, F) Comparison of rmFLIM images of liver sections with and without dPGS-ICC (+dPGS-ICC and -dPGS-ICC) morphologically corresponding to part D. Color coding is based on the amplitude ratio a_1/a_2 of a global lifetime fit with three components ($\tau_1 = 0.27$ ns, $\tau_2 = 1.1$ ns, $\tau_3 = 3.5$ ns). The dPGS-ICC fluorescence signature (red) is located in areas of sinusoids in a patchy pattern, consistent with Kupffer cells (see the Supporting Information). Fluorescence excitation was at 485 nm; emission was detected with a band-pass filter HQ_{620/60} nm. Scale bar: 40 μ m.

where the excited state is rapidly relaxed by *cis*–*trans* photoisomerization occurring in the polymethine linker.²⁰ The 1.1 ns lifetime probably arises from ICC molecules in which rotation about the

polymethine linkage of the fluorophore is constrained.²¹ In our case, the constrained rotation is mediated by interaction with the polyglycerol branches of the nanocarrier. Thus, the interaction of ICC dyes with the nanocarrier matrix results in an additional longer fluorescence lifetime with an amplitude ratio (a_1/a_2) between the two lifetime species of about 6.

For FLIM measurements we used paraffin embedded liver sections from rats previously injected (iv) with dPGS-ICC. A control sample from untreated rats was also prepared. Liver tissue is known for its autofluorescence.²² Figure 5A shows the autofluorescence of liver tissue under conditions of fluorescence excitation and emission used for the detection of ICC in our FLIM setup. A corresponding histological micrograph (Haematoxylin and eosin stain) is provided in Figure 5B. A FLIM image of a liver section with dPGS-ICC is shown in Figure 5C. The time-resolved autofluorescence data in the FLIM image of liver sections without dPGS-ICC were best fitted by using three exponentials with peaks in the lifetime histogram at about 0.27, 1.1, and 3.5 ns (see the Supporting Information). As the two shortest lifetime species (0.27 and 1.1 ns) extracted from the liver autofluorescence are in the same range as the two lifetimes of dPGS-ICC, a “lifetime only”-based localization of dPGS-ICC is not feasible. To discriminate the ICC fluorescence against the autofluorescent background, we color-coded the FLIM images according to the amplitude ratio of the two shortest lifetime components (a_1/a_2) from the global fit. The a_1/a_2 -value of the autofluorescent background ranges from about 0.5 to 4.5. The amplitude ratio (a_1/a_2) for the two lifetime species of dPGS-ICC is about 6. As a threshold we used 5, which corresponds to 80% and 16% relative amplitude of the 0.27 and 1.1 ns lifetime species, respectively. Amplitude ratio values above 5, indicating dPGS-ICC, are colored in red. Amplitude ratio values between 0.5 and 5 indicate autofluorescent background and are colored in blue. The rmFLIM images in Figure 5E and F allow a clear-cut discrimination between autofluorescent background and the localization of the dPGS-ICC in the liver tissue. While in the control liver sections a predominantly homogeneous blue coloring is visible (Figure 5E), the localization of the dPGS-ICC nanocarriers in red shows a patchy pattern in the liver sinusoids (Figure 5F, see the Supporting Information). This pattern is virtually identical with the distribution of Kupffer cells (Figure 5D), a phagocytically competent cell type.

In summary, we have shown that a consequent application of the FLIM analysis capabilities in the version of rmFLIM together with the unique fluorescence lifetime features of the target molecule allows for an easy and fast localization of the target molecule in the cellular context or within tissues. We note that for receptor–ligand complexes the specific binding of the ligand can be observed directly after addition of the fluorescently labeled ligand without any further washing or purification steps, as the ratiometric approach allows for effective background suppression.

■ ASSOCIATED CONTENT

S Supporting Information. Experimental methods and detailed results. This material is available free of charge via the Internet at <http://pubs.acs.org>.

■ AUTHOR INFORMATION

Corresponding Author

*E-mail: alexiev@physik.fu-berlin.de.

■ ACKNOWLEDGMENT

This work was supported partly by Sfb449 (DFG) to U.A. and by STE 477/9-1 (DFG) and MedSys 0101-31P5783 (BMBF) to C.S.

■ ABBREVIATIONS

GPCR, G-protein coupled receptor; rmFLIM, ratiometric fluorescence lifetime imaging microscopy; FRET, Förster resonance energy transfer; Flu, fluorescein; Cys-Flu, fluorescein bound to cysteine; Opsin-Cys316-Flu, fluorescein bound to Cys316 in the opsin molecule; MOR, μ -opioid receptor; NLX, naloxone; NLX-Flu, naloxone coupled to fluorescein; dPGS, dendritic polyglycerolsulfate; ICC, indocarbocyanine dye; dPGS-ICC, ICC coupled to dPGS

■ REFERENCES

- (1) Festy, F.; Ameer-Beg, S. M.; Ng, T.; Suhling, K. Imaging proteins in vivo using fluorescence lifetime microscopy. *Mol. Biosyst.* **2007**, *3* (6), 381–91.
- (2) Kenworthy, A. K. Imaging protein-protein interactions using fluorescence resonance energy transfer microscopy. *Methods* **2001**, *24* (3), 289–96.
- (3) Verveer, P. J.; Wouters, F. S.; Reynolds, A. R.; Bastiaens, P. I. Quantitative imaging of lateral Erbb1 receptor signal propagation in the plasma membrane. *Science* **2000**, *290* (5496), 1567–70.
- (4) Giepmans, B. N.; Adams, S. R.; Ellisman, M. H.; Tsien, R. Y. The fluorescent toolbox for assessing protein location and function. *Science* **2006**, *312* (5771), 217–24.
- (5) Daly, C. J.; McGrath, J. C. Fluorescent ligands, antibodies, and proteins for the study of receptors. *Pharmacol. Ther.* **2003**, *100* (2), 101–18.
- (6) Alonso, D.; Vazquez-Villa, H.; Gamo, A. M.; Martinez-Esperon, M. F.; Tortosa, M.; Viso, A.; Fernandez de la Pradilla, R.; Junquera, E.; Aicart, E.; Martin-Fonterech, M.; Benhamu, B.; Lopez-Rodriguez, M. L.; Ortega-Gutierrez, S. Development of fluorescent ligands for the human 5-HT1a receptor. *ACS Med. Chem. Lett.* **2010**, *1* (6), 249–253.
- (7) Middleton, R. J.; Kellam, B. Fluorophore-tagged GPCR ligands. *Curr. Opin. Chem. Biol.* **2005**, *9* (5), 517–25.
- (8) Nomura, W.; Tanabe, Y.; Tsutsumi, H.; Tanaka, T.; Ohba, K.; Yamamoto, N.; Tamamura, H. Fluorophore labeling enables imaging and evaluation of specific CXCR4-ligand interaction at the cell membrane for fluorescence-based screening. *Bioconjugate Chem.* **2008**, *19* (9), 1917–20.
- (9) Doose, S.; Neuweiler, H.; Sauer, M. Fluorescence quenching by photoinduced electron transfer: reporter for conformational dynamics of macromolecules.
- (10) Alexiev, U.; Rimke, I.; Pohlmann, T. Elucidation of the nature of the conformational changes of the EF-interhelical loop in bacteriorhodopsin and of the helix VIII on the cytoplasmic surface of bovine rhodopsin: a time-resolved fluorescence depolarization study. *J. Mol. Biol.* **2003**, *328* (3), 705–19.
- (11) Kim, T. Y.; Moeller, M.; Winkler, K.; Kirchberg, K.; Alexiev, U. Dissection of environmental changes at the cytoplasmic surface of light-activated bacteriorhodopsin and visual rhodopsin: sequence of spectrally silent steps. *Photochem. Photobiol.* **2009**, *85* (2), 570–7.
- (12) Kirchberg, K.; Kim, T. Y.; Haase, S.; Alexiev, U. Functional interaction structures of the photochromic retinal protein rhodopsin. *Photochem. Photobiol. Sci.* **2010**, *9*, (2), 226–33.
- (13) Kim, T. Y.; Winkler, K.; Alexiev, U. Picosecond multidimensional fluorescence spectroscopy: a tool to measure real-time protein dynamics during function. *Photochem. Photobiol.* **2007**, *83* (2), 378–84.
- (14) Arden, J. R.; Segredo, V.; Wang, Z.; Lameh, J.; Sadee, W. Phosphorylation and agonist-specific intracellular trafficking of an epitope-tagged mu-opioid receptor expressed in HEK 293 cells. *J. Neurochem.* **1995**, *65* (4), 1636–45.
- (15) Zöllner, C.; Stein, C. Opioids. *Handb. Exp. Pharmacol.* **2007**, No. 177, 31–63.
- (16) Knapp, R. J.; Malatynska, E.; Collins, N.; Fang, L.; Wang, J. Y.; Hruby, V. J.; Roeske, W. R.; Yamamura, H. I. Molecular biology and pharmacology of cloned opioid receptors. *FASEB J.* **1995**, *9* (7), 516–25.
- (17) Ge, X.; Qiu, Y.; Loh, H. H.; Law, P. Y. GRIN1 regulates micro-opioid receptor activities by tethering the receptor and G protein in the lipid raft. *J. Biol. Chem.* **2009**, *284* (52), 36521–34.
- (18) Khandare, J.; Mohr, A.; Calderon, M.; Welker, P.; Licha, K.; Haag, R. Structure-biocompatibility relationship of dendritic polyglycerol derivatives. *Biomaterials* **2010**, *31*, (15), 4268–77.
- (19) Dernedde, J.; Rausch, A.; Weinhart, M.; Enders, S.; Tauber, R.; Licha, K.; Schirner, M.; Zuegel, U.; Bonin, A.; Haag, R. Dendritic polyglycerols as multivalent inhibitors of inflammation. *Proc. Natl. Acad. Sci. U.S.A.* **2010**, *107*, 19697–48.
- (20) Chibisov, A. K.; Zakharyova, G. V.; Goerner, H.; Sogulyaev, Y. A.; Mushkalo, I. L.; Tolmachev, A. I. Photorelaxation processes on covalently linked indocarbocyanine and thiocarbocyanine dyes. *J. Phys. Chem.* **1995**, *99* (3), 886–893.
- (21) Iqbal, A.; Arslan, S.; Okumus, B.; Wilson, T. J.; Giraud, G.; Norman, D. G.; Ha, T.; Lilley, D. M. Orientation dependence in fluorescent energy transfer between Cy3 and Cy5 terminally attached to double-stranded nucleic acids. *Proc. Natl. Acad. Sci. U.S.A.* **2008**, *105* (32), 11176–81.
- (22) Croce, A. C.; De Simone, U.; Vairetti, M.; Ferrigno, A.; Boncompagni, E.; Freitas, I.; Bottiroli, G. Liver autofluorescence properties in animal model under altered nutritional conditions. *Photochem. Photobiol. Sci.* **2008**, *7* (9), 1046–53.